Optics Letters

# Femtosecond laser-inscribed fiber interface Mach–Zehnder interferometer for temperature-insensitive refractive index measurement

YUNFANG ZHANG, CHUPAO LIN, CHANGRUI LIAO,* KAIMING YANG, ZHENGYONG LI, AND YIPING WANG

*Key Laboratory of Optoelectronic Devices and Systems of Ministry of Education and Guangdong Province, College of Optoelectronic Engineering, Shenzhen University, Shenzhen 518060, China*
**Corresponding author: cliao@szu.edu.cn*

*Received 30 April 2018; revised 4 August 2018; accepted 14 August 2018; posted 20 August 2018 (Doc. ID 330537); published 11 September 2018*

**A new fiber interface Mach–Zehnder interferometer has been fabricated, to the best of our knowledge, in coreless fiber by femtosecond laser-inscription for temperature-insensitive refractive index measurement. A straight waveguide was inscribed along the central axis of the coreless fiber as the reference arm, and the other curved waveguide (interface waveguide) was then inscribed bending toward the cladding interface to obtain a strong evanescent field sensitive to ambient refractive index. This fiber interface Mach–Zehnder interferometer exhibits a high refractive index (RI) sensitivity of ∼3000 nm/RIU at an RI value of 1.432. Moreover, with the significant advantages of high mechanical strength and temperature independence, such a fiber Mach–Zehnder interferometer may find many potential applications in biochemical sensing.** 

***OCIS codes:*** (050.6875) Three-dimensional fabrication; (130.2755) Glass waveguides; (240.6690) Surface waves; (060.2370) Fiber optics sensors.

https://doi.org/10.1364/OL.43.004421

A femtosecond laser-inscribing waveguide is an efficient and flexible method to fabricate three-dimensional (3D) optical circuits in bulk glasses, which has been successfully extended to inscribe waveguides in the cladding of optical fiber [1–3]. With the advantages of an all-fiber structure, excellent mechanical strength, and simple fabrication, several in-fiber waveguide devices designed for sensing have recently been proposed and fabricated by a femtosecond laser in single-mode fibers (SMFs). In 2017, Lin *et al.* reported a fiber surface Bragg-grating waveguide-based refractive index (RI) sensor, which used a femtosecond laser-inscribed waveguide across the fiber core to couple the light from the core to the fiber surface [4]. Li *et al.* demonstrated an in-fiber Mach–Zehnder interferometer (MZI) for strain measurement [5]. Pallarés-Aldeiturriaga *et al.* designed an in-fiber Mach–Zehnder interferometer as a curved sensor [6].

In this Letter, we demonstrate a fiber interface MZI sensor, which is fabricated in a coreless fiber spliced between two SMFs by femtosecond laser inscription. As shown in Fig. 1, as the reference arm, a straight waveguide ($W_S$) inscribed along the central axis of the coreless fiber guides the light directly from the lead-in SMF to the lead-out SMF. As the sensing arm, a curved waveguide ($W_C$) couples the light from the lead-in SMF to the fiber interface and then back to the lead-out SMF, which creates a strong evanescent field that is sensitive to the ambient RI. Such a fiber interface MZI exhibits an RI sensitivity of ∼3000 nm/RIU at the RI value of 1.432. In addition, compared with other fiber RI sensors, i.e., long-period fiber grating [7], title fiber grating [8], fiber microcavity devices [9], tapered fibers [10,11] etc., this fiber interface MZI is hardly sensitive to temperature, which is important in RI measurement. Such a fiber interface MZI exhibits a high RI sensitivity, high mechanical strength, and little temperature cross-sensitivity and may find applications in biochemical sensing.

The schematic diagram of the fiber interface MZI is shown in Fig. 1. The light propagating in $SMF_1$ is split into two beams, denoted as $I_1$ and $I_2$, respectively, in the coreless fiber. $I_1$ propagates along the $W_S$, and $I_2$ enters into the $W_C$. The two light beams recombine at $SMF_2$, resulting in an interference pattern. The output intensity of MZI can be described as

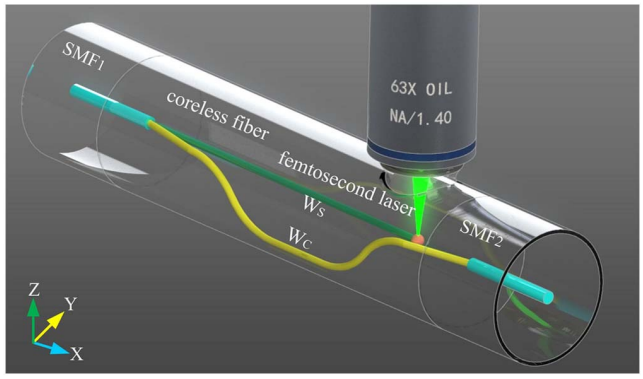


**Fig. 1.** Schematic diagram of a femtosecond laser-inscribed fiber interface waveguide MZI.

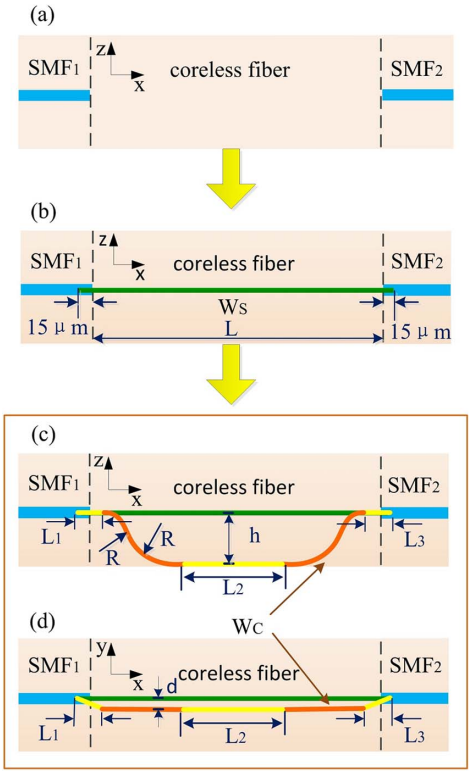


**Fig. 2.** Flow chart of device fabrication. (a) The coreless fiber is spliced between two SMFs. (b) The $W_S$ is inscribed along the central axis of the coreless fiber. (c), (d) The $W_C$ is inscribed in the coreless fiber from the side view and top view. The optimized parameters: $L_1 = 0.5$ mm, $d = 6$ μm, $h = 60$ μm, $R = 50$ mm.

$$I = I_1 + I_2 + 2\sqrt{I_1 I_2}\cos(2\pi\Delta(nL)/\lambda), \quad (1)$$

where $\lambda$ is the wavelength and $\Delta(nL)$ is the optical path difference (OPD) between the two interferometer arms. When the condition $2\pi\Delta(nL)/\lambda = (2m+1)\pi$ is satisfied, where $m$ is an integer, the intensity dip appears at the wavelength

$$\lambda_{\text{dip}} = 2\Delta(nL)/(2m+1). \quad (2)$$

The free spectral range (FSR) of the interference fringe dip of interest is determined by the OPD, $\Delta(nL)$, as

$$\text{FSR} = \lambda^2/(\Delta(nL)). \quad (3)$$

The flow chart of device fabrication is shown in Fig. 2. First, a section of coreless fiber is spliced between two SMFs (Corning, SMF-28) by a commercial fusion splicer (Fujikura FSM-60s), which supplies a platform for waveguide inscription, as shown in Fig. 2(a). Second, the $W_S$ is inscribed from the core of $SMF_1$ to the core of $SMF_2$ through the coreless fiber, as shown in Fig. 2(b). To increase the coupling efficiency between the straight waveguide and the connected SMFs, $W_S$ is stretched into the cores of the SMFs with a length of ~15 μm. A femtosecond laser (PHAROS, 532 nm/250 fs/200 kHz) is employed to inscribe the waveguide, and an oil-immersed objective lens (NA = 1.4) is selected to eliminate the aberration caused by the cylindrical morphology of fiber. The fixed fiber is translated relative to the focused laser beam by use of a 3D air-bearing motion stage (Aerotech). The single-pulse energy of the femtosecond laser is optimized as ~120 nJ, and the translation velocity of the fiber is set to be 0.2 mm/s. The propagation loss of the inscribed waveguide and the coupling loss at the joint point have been measured by the cut-back method, and the result is shown in Fig. 3, where the optimized propagation loss of ~0.1 dB/mm and the coupling loss of ~0.6 dB have been achieved. Reducing the loss of the inscribed waveguide is the foundation of high-quality fiber interface MZI fabrication.

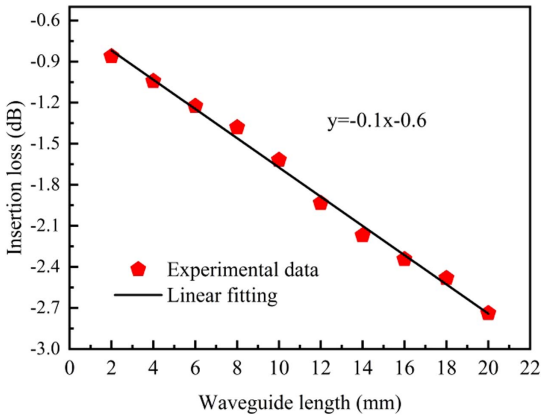


**Fig. 3.** Relationship between the insertion loss and the waveguide length of the waveguide inscribed in the coreless fiber at 1550 nm.

Third, as shown in Figs. 2(c) and 2(d), the 3D $W_C$ is inscribed in the side of the $W_S$, and can be divided into two s-bend waveguides ($S_1$, $S_2$) and three linear waveguides ($L_1$, $L_2$, $L_3$). To enhance the evanescent field of the $W_C$, the linear waveguide ($L_2$), which is named as fiber interface waveguide, is inscribed very close to the interface of the fiber cladding by precisely focusing the femtosecond laser beam on the bottom surface of the fiber. To avoid cross talk between the $W_C$ and $W_S$, the s-bend waveguides ($S_1$, $S_2$) are inscribed far from the $W_S$, at a distance (d) of ~6 μm, and are connected to the cores of the SMF using two straight waveguides ($L_1$ and $L_3$, respectively). To decrease the total loss of the fiber interface MZI, the following parameters have been optimized: the curvature radius (R) of s-bend waveguides is 50 mm and the distance ($h$) between the $W_S$ and $W_C$ is 60 μm.

The optical microscopy image of the fiber interface MZI is shown in Fig. 4(a). The $W_S$ is inscribed across the core axis of the coreless fiber, and the $W_C$ is bent slightly toward the interface of the coreless fiber. From the cross sectional morphology shown in Fig. 4(b), it can be seen that the $W_C$ completely approaches the interface of the coreless fiber; the distance between $W_C$ and $W_S$ is ~6 μm in the horizontal direction and ~60.5 μm in the vertical direction, and the size of these two waveguides are ~14 μm in depth and ~3 μm in width.

To observe the intensity ratio of the MZI, the mode field of the waveguide was measured. Light from a tunable laser (Agilent, Model 81940A) with a wavelength range from 1520 to 1620 nm was launched into the MZI and collected by a camera (Newport, LBP2-HR-IR2). As shown in Fig. 4(c), the light intensities in the two waveguides are almost the same, and the mode profile of the $W_C$ (9.22 μm × 8.56 μm) is slightly smaller than that of the $W_S$ (9.88 μm × 8.99 μm), which may—due to the dramatic RI difference between the

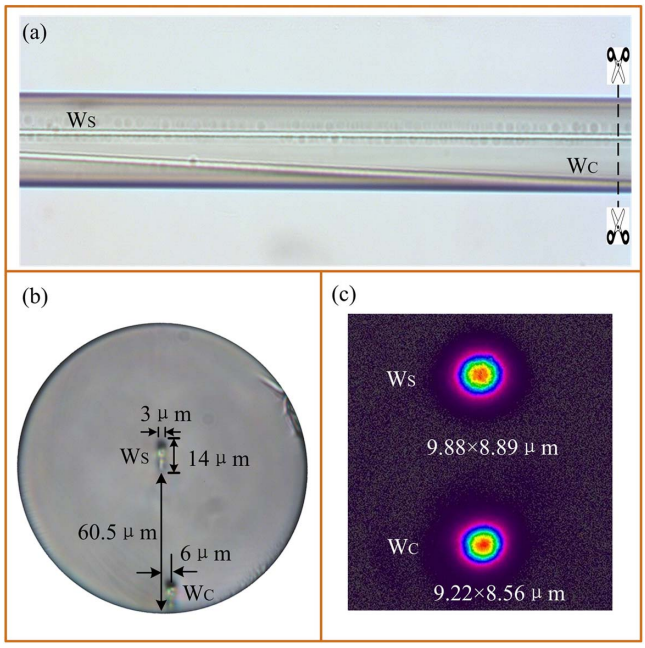


**Fig. 4.** (a) Optical microscope image of fiber interface MZI with $W_S$ and $W_C$ inscribed by the femtosecond laser. (b) Morphology of the fiber end face at the cut point in (a). The $W_C$ is close to the coreless fiber interface. (c) Mode profile of the two waveguides ($W_S$ and $W_C$) at 1560 nm.

air and interface waveguide—cause the $W_C$ to confine the light better and exhibit a smaller effective mode RI than $W_S$.

As indicated in Eq. (3), the FSR varies inversely with the length of the interface waveguide ($L_2$), and therefore the value of FSR can be optimized by adjusting the length of the interface waveguide at a given wavelength. Three fiber interface MZIs with interface waveguide lengths of 6.988, 10.465, and 12.030 mm have been successfully fabricated, and the corresponding transmission spectra are shown in Fig. 5, from which it can be seen that with an increase of interface waveguide length, the total length difference between the $W_S$ and $W_C$ is unchanged, but the value of FSR decreases. This phenomenon confirms that the mode effective RI of the interface

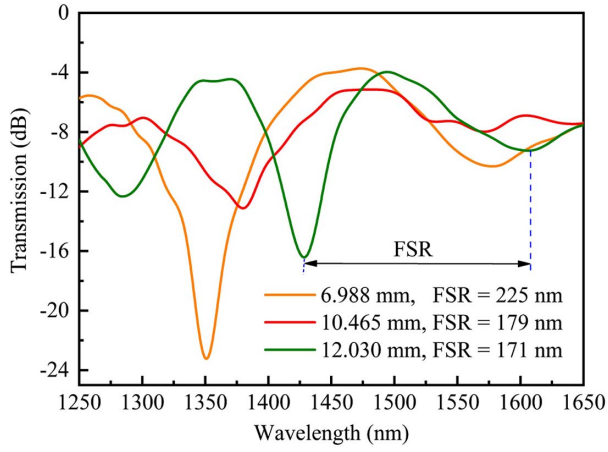


**Fig. 5.** Transmission spectra and FSR values of the fiber interface MZIs with different interface waveguide lengths ($L_2$).

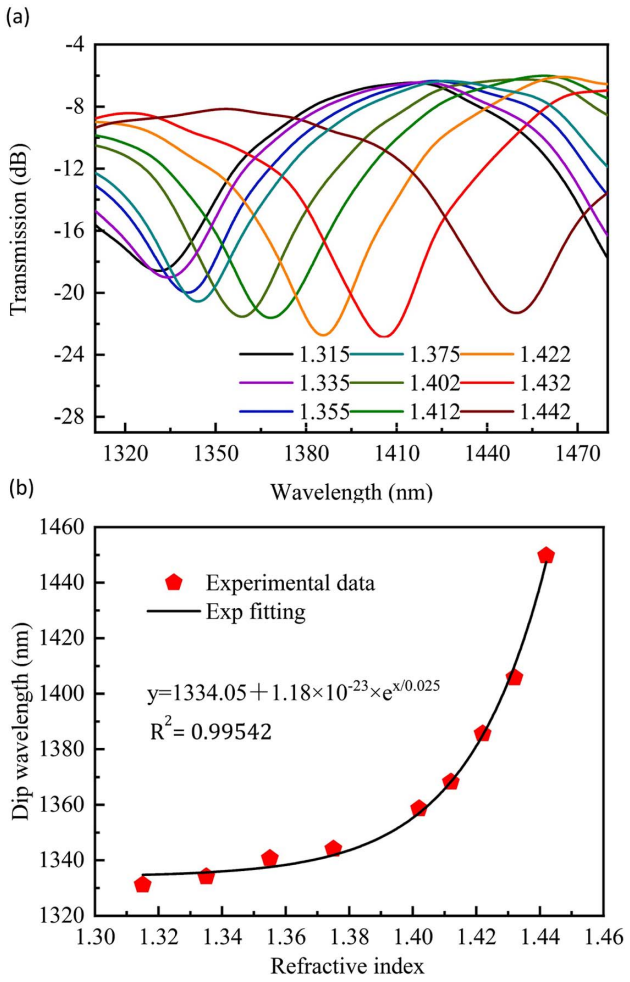


**Fig. 6.** Liquid RI response of the fiber interface MZI. (a) Transmission spectra of the fiber interface MZI immersed in different RI liquids. (b) Exponential fitting relationship between the wavelength of the traced interference dip and the RI of liquid.

waveguide is different from that of the waveguide inscribed inside the fiber.

The RI response of the fiber interface MZI ($L_2 = 10.430$ mm) was investigated at room temperature by immersing it in a series of standard RI liquids (Cargille Labs) whose RI value increased from 1.315 to 1.442. After each test, the device was carefully cleaned with alcohol to remove the residual liquid by observing the restoration of the original spectrum. The measured RI response of the fiber interface MZI is shown in Fig. 6, where the interference dip exhibits a significant redshift with an increase of liquid RI and an exponential fitting method has been employed to reveal the RI response of the traced dip. It is noted that the evanescent field of the $W_C$ can be enhanced as the RI of the liquid approaches that of the fiber cladding, and therefore a high sensitivity of ~3000 nm/RIU can be achieved when the tested liquid RI is ~1.432. Moreover, the full width at half-maximum value of the resonance is measured to be ~45 nm, and a signal-to-noise ratio is assumed to be 60 dB, so the accuracy and resolution of this fiber interface MZI can be calculated of $3.2 \times 10^{-4}$ RIU and $3.3 \times 10^{-6}$ RIU, respectively [12,13].

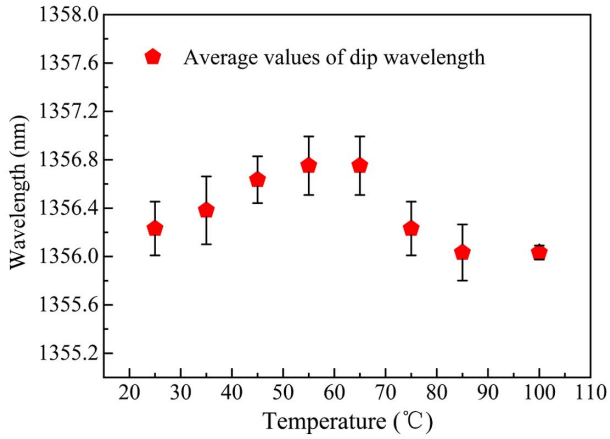


**Fig. 7.** Relationship of the average and variance values of the traced interference dip wavelength and ambient temperature.

The temperature influence on the fiber interface MZI ($L_2 = 6.988$ mm) was also investigated by placing it in an electric oven in air and gradually changing the temperature between 25°C and 100°C. The average and variance values of the traced dip wavelength are illustrated in Fig. 7, and there is only a tiny wavelength fluctuation of ~0.6 at ~1356.4 nm that may result from measurement error, which can be neglected in RI measurement.

In Eq. (2), the temperature response of the fiber interface MZI is relevant to the OPD of $W_S$ and $W_C$. Because these two waveguides were inscribed in the same material by use of the same fabrication parameters, they have the identical thermo-optical and thermal expansion coefficients. Due to the curvature radius of s-bend waveguides being very large, the length of $W_C$ can be approximately equal to that of $W_S$. Therefore, the OPD between these two waveguides is independent on ambient temperature, and the interference dip hardly shifts in temperature measurement.

In conclusion, a new fiber interface MZI has been successfully fabricated, to the best of our knowledge, in the interface of coreless fiber by femtosecond laser direct writing for a temperature-insensitive refractive index measurement. To obtain a low-loss waveguide, the pulse energy of a femtosecond laser is optimized at ~120 nJ, and the translation velocity of the fiber is set to 0.2 mm/s. An optimized propagation loss of ~0.1 dB/mm and a coupling loss of ~0.6 dB have been achieved. A straight waveguide is first inscribed in the center axis of the coreless fiber as a reference arm. A curved waveguide is fabricated in the coreless fiber interface to obtain a strong evanescent field that is sensitive to the ambient refractive index. The fiber interface MZI exhibits a high sensitivity of ~3000 nm/RIU at an RI value of ~1.432. It is worth noting that the fiber interface MZI has little response to temperature in wavelength, because these two interference arms were inscribed in the same material and have minute difference of their length, and thus the OPD is independent on the ambient temperature. With the significant advantages of temperature independence and high mechanical strength, such a fiber interface MZI may find many potential applications in biochemical sensing.

**Funding.** National Natural Science Foundation of China (NSFC) (61575128, 61425007, 61635007); Natural Science Foundation of Guangdong Province (2015B010105007, 2014A030308007); Science and Technology Innovation Commission of Shenzhen (JCYJ20160520163134575, JCYJ20160427104925452, KQJSCX20170727101953680); Development and Reform Commission of Shenzhen Municipality Foundation.

## REFERENCES

1. P. R. Herman, K. H. Y. Cheng, J. R. Grenier, M. Haque, and K. K. C. Lee, MATEC Web Conf. **8**, 05010 (2013).
2. M. Haque, K. K. Lee, S. Ho, L. A. Fernandes, and P. R. Herman, Lab Chip **14**, 3817 (2014).
3. J. R. Grenier, L. A. Fernandes, and P. R. Herman, Opt. Express **23**, 16760 (2015).
4. C. Lin, C. Liao, J. Wang, J. He, Y. Wang, Z. Li, T. Yang, F. Zhu, K. Yang, Z. Zhang, and Y. Wang, Opt. Lett. **42**, 1684 (2017).
5. W. W. Li, W. P. Chen, D. N. Wang, Z. K. Wang, and B. Xu, Opt. Lett. **42**, 4438 (2017).
6. D. Pallarés-Aldeiturriaga, L. Rodríguez-Cobo, A. Quintela, and J. M. López-Higuera, J. Lightwave Technol. **35**, 4624 (2017).
7. C. L. Fu, X. Y. Zhong, C. R. Liao, Y. P. Wang, Y. Wang, J. Tang, S. Liu, and Q. Wang, IEEE Photon. J. **7**, 1 (2015).
8. T. Wang, K. Liu, J. Jiang, M. Xue, P. Chang, and T. Liu, Opt. Express **25**, 14900 (2017).
9. Z. Li, C. Liao, Y. Wang, X. Dong, S. Liu, K. Yang, Q. Wang, and J. Zhou, Opt. Lett. **39**, 4982 (2014).
10. P. Lu, L. Men, K. Sooley, and Q. Chen, Appl. Phys. Lett. **94**, 131110 (2009).
11. L. Xu, Y. Li, and B. Li, Appl. Phys. Lett. **101**, 153510 (2012).
12. I. M. White and X. D. Fan, Opt. Express **16**, 1020 (2008).
13. Y. Wang, M. W. Yang, D. N. Wang, S. J. Liu, and P. X. Lu, J. Opt. Soc. Am. B **27**, 370 (2010).